Quadrature-Averaged Homodyne Detection for Estimating Cavity Parameters

Giada R. La Gala,[1] Arvind Shankar Kumar,[2] Rick Leijssen,[1] Ewold Verhagen,[1] and Juha T. Muhonen[2,*]

[1] *Center for Nanophotonics, AMOLF, Science Park 104, Amsterdam 1098 XG, Netherlands*

[2] *Department of Physics and Nanoscience Center, University of Jyväskylä, P.O. Box 35, University of Jyväskylä FI-40014, Finland*

(Received 13 September 2022; revised 13 April 2023; accepted 4 May 2023; published 2 June 2023)

Balanced homodyne interferometry is a well-known detection technique that allows for sensitive characterization of light fields. Conventionally a homodyne interferometer is operated by locking the relative phase of a reference beam to the signal beam by means of an active feedback loop. A less often used method is to perform a slow continuous modulation of the reference beam arm length that corresponds to averaging all relative phases during the measurement. Here we show theoretically and experimentally that this quadrature averaging can be advantageous in estimating the parameters of a resonant optical cavity. We demonstrate that the averaging turns the transduction function, from cavity frequency fluctuations into the interferometer signal, into a simple function of the laser detuning that, notably, does not depend on the parameters of possible nonresonant channels present in the system. The method needs no active feedback and gives results that are easy to interpret. Moreover, the phase-averaged measurement allows characterization of the absolute magnitude of a cavity frequency modulation.

DOI: 10.1103/PhysRevApplied.19.064006

I. INTRODUCTION

Balanced homodyne interferometry (BHI) offers a unique tool to characterize arbitrary quadratures of a light field with photon shot-noise-limited sensitivity, and is in use in fields varying from detection of gravitational waves [1] to quantum applications of cavity optomechanics [2]. A common use case for BHI is to probe an optical cavity that is located in one of the arms of the interferometer (called the signal arm). Any frequency changes of that optical cavity are transferred into relative phase differences between the two interferometer arms (signal and local oscillator). Of note, the induced phase difference is also enhanced by the cavity finesse.

Usually the detection of the phase difference is performed by locking the local oscillator arm phase with regards to the (nonperturbed) signal phase by means of a variable path length (piezomirror, fiber stretcher etc.) [3]. In this way a particular quadrature of the light field can be measured [4]. This obviously assumes that the signal to be measured is at a much higher frequency than the locking bandwidth in order for the feedback not to cancel out the signal. In addition, the actual angle of the interferometer is generally not an accessible observable and hence "locking the angle" is usually accomplished by locking the dc signal of the interferometer output. As we show below, this can actually lead to unwanted side effects for the measurement if the signal also includes a nonresonant background.

One method used to avoid the effects of the nonresonant channels is to convert the homodyne signal into a "pseudo-heterodyne" signal by modulating the local oscillator path with a frequency ω_1 [5]. This will create sidebands for the detected signal at frequencies separated from the original detection frequency by ω_1 allowing separating the interferometer signal from the background signals. This method has, for example, been applied in scanning near-field optical microscopes [6–8]. In this method ω_1 needs to be much larger than the measurement bandwidth around the signal to be detected so that well-defined sidebands are created.

A less often used method, that we focus on here, is to average over all possible phases of the local oscillator by modulating the local oscillator slowly, i.e., with a much lower frequency than the bandwidth of the measurement. This modulation will then not create sidebands but rather average over all the possible angles during the homodyne measurement [9–11]. Here we show that this quadrature-averaged BHI can be a useful method in characterizing optical cavities when the measured signal also includes light that has not interacted with the cavity (nonresonant reflection or transmission). This has applications especially in cavity optomechanics [12], and in other areas using nanophotonic cavities, where the nonresonant channels can be sensitive to the experimental conditions [13–21]. In a conventional locked homodyne measurement

*juha.t.muhonen@jyu.fi

the interference with the resonant and nonresonant part generally leads to a Fano-shaped resonance from which the parameters of the cavity can be hard to extract. Additionally, the homodyne interferometer angle will vary as a function of the detuning of the laser and the optical cavity. We show that by using quadrature-averaged BHI we can avert both of these problems. A simple Lorentzian shape for the resonance is recovered, allowing easier interpretation, and the variation in the measurement angle with laser detuning is eliminated. Moreover, the quadrature-averaged BHI allows extracting the absolute magnitude of the cavity frequency modulation by comparing the different harmonic components. This can then be used to retrieve, e.g., the thermal modulation amplitude of an optomechanical resonator without any further calibration.

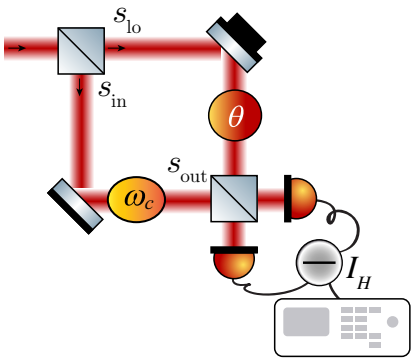

FIG. 1. Schematic of a homodyne interferometer. Symbols are defined in the main text.

II. BACKGROUND: HOMODYNE INTERFEROMETRY IN THE PRESENCE OF NONRESONANT CHANNELS

A. Homodyne interferometer description

In Fig. 1 we show a schematic of a balanced homodyne interferometer. We assume that the signal and the local oscillator arms are described by linearly polarized coherent states with complex parameters $s_{\rm in} = |s_{\rm in}|\, e^{i\phi_{\rm in}}$ and $s_{\rm lo} = |s_{\rm lo}|\, e^{i\phi_{\rm lo}}$. By changing the local oscillator arm length, the phase $\phi_{\rm lo}$ can be tuned and a relative phase difference θ is imprinted between the two paths. By convention, we normalize all fields s_i such that $|s_i|^2$ is the photon flux in beam i and hence the power in the beam is $P_i = \hbar\omega_l |s_i|^2$, where ω_l is the frequency of the light. The optical cavity under study (with resonance frequency ω_c) is placed on the signal arm and due to interaction with the cavity system, the signal beam $s_{\rm in}$ is transformed into the output beam $s_{\rm out} = r s_{\rm in}$, where r is the *transfer function* describing the cavity system. Subsequently the two beams are interfered at the final 50:50 beam splitter leading to outputs $s_+ = 1/\sqrt{2}(i s_{\rm out} + s_{\rm lo})$ and $s_- = 1/\sqrt{2}(i s_{\rm lo} + s_{\rm out})$, which are detected by separate photodiodes. The two output currents are then subtracted. The measured subtracted photocurrent from the detector (I_H) can be written as

$$\begin{aligned} I_H &= |s_+|^2 - |s_-|^2 = s_+^\star s_+ - s_-^\star s_- \\ &= i(s_{\rm lo}^\star s_{\rm out} - s_{\rm out}^\star s_{\rm lo}) \\ &= -2\,|s_{\rm in}|\,|s_{\rm lo}|\,(\mathrm{Im}(r)\cos\theta - \mathrm{Re}(r)\sin\theta)\,, \end{aligned} \tag{1}$$

where $\theta = \phi_{\rm lo} - \phi_{\rm in}$ is the phase difference between the two arms of the interferometer and $\mathrm{Re}(r)$ and $\mathrm{Im}(r)$ are the real and imaginary parts of the cavity transfer function, respectively. (Note that changing the convention to $\theta = \phi_{\rm in} - \phi_{\rm lo}$ would change the sign in front of the sine term.) We neglect any gain or loss factor depending on the quantum efficiencies of the detectors, the amplifier gain and other electronic properties; these would simply lead to a constant multiplier for this term. Varying θ between 0 and 2π (by tuning $\phi_{\rm lo}$) corresponds to choosing a specific quadrature of the field: where $\theta = 0, \pi$ and $\theta = \pm\pi/2$ are the extreme cases usually known as the *phase quadrature* and the *amplitude quadrature*. These are orthogonal quantities in the optical phase space.

B. Input-output description of a cavity system

The beam $s_{\rm out}$ carries information about the cavity system. For a single-mode, high-finesse cavity, the transfer function can be described by a general resonant response [22]

$$\begin{aligned} r &= c e^{i\varphi} - \frac{\eta\kappa}{\kappa/2 + i(\omega_c - \omega)} \\ &= c e^{i\varphi} - \frac{2\eta}{1 + i\Delta_n}, \end{aligned} \tag{2}$$

where $\Delta \equiv \omega_c - \omega$ is the detuning of the incident laser frequency ω from the cavity resonance frequency ω_c and we introduce a normalized detuning parameter $\Delta_n = 2\Delta/\kappa$. The first term in this general expression describes a nonresonant channel, with amplitude c and phase φ, e.g., a direct reflection of light that does not enter the cavity. The second term describes the cavity resonance, which is characterized by the resonance frequency ω_c, cavity decay rate κ and radiative coupling efficiency $\eta \equiv \kappa_{\rm ex}/\kappa$ where $\kappa_{\rm ex}$ is both the decay rate through the radiative coupling channel, i.e., radiated into the beam $s_{\rm out}$, and the coupling from the input channel to the cavity (assumed equal). We note that in the most general case, the transfer function could still be multiplied by an overall phase factor, but any global phase factor can always be absorbed into a proper adjustment of the phase θ when evaluating the resulting homodyne signal.

It is also useful to write down the normalized transfer function that is unity at resonance (without the nonresonant

part)

$$r_n \equiv \frac{r}{2\eta} = c_n e^{i\varphi} - \frac{1}{1+i\Delta_n}, \tag{3}$$

where $c_n = c/(2\eta)$ is the normalized c that will appear in all formulae below. We note that the case $c = 1, \varphi = 0$, corresponds to the classical time average of the famous input-output expression of $s_{\text{out}} = s_{\text{in}} - \sqrt{\kappa_{ex}}s$, where s is the field inside the cavity.

From Eq. (1) we see that specific homodyne angles ideally probe the real or imaginary part of the cavity response, given by

$$\text{Re}(r_n) = c_n \cos\varphi - \frac{1}{1+\Delta_n^2}, \tag{4}$$

$$\text{Im}(r_n) = c_n \sin\varphi + \frac{\Delta_n}{1+\Delta_n^2}. \tag{5}$$

In general, depending on the system characteristics (the number of coupling channels, the relative loss rates, relative phases) the resonant lineshapes as a function of Δ can vary strongly. This can be understood as a Fano interference effect [23], as it arises due to the interference of the resonant and the direct (broadband) channel between input and output. This is important for experiments as the amplitude and phase of the non-resonant part can be very sensitive to the experimental conditions in such way that the detuning dependence of a specific quadrature is strongly affected by small changes in the experimental conditions [14,16–19].

To illustrate the effect of the nonresonant channel, we plot in Fig. 2 the phase and amplitude (and the real and imaginary parts separately) of the transfer function as a function of detuning for three particular cases: (i) a *single-sided* cavity ($c = 1$, $\varphi = 0$, $\eta = 1$), where all the light in the cavity is returned towards the detector, (ii) a *double-sided* cavity ($c = 1$, $\varphi = 0$, $\eta = 0.5$), where half the light is lost due to some other channels (i.e., critical coupling), and (iii) a double-sided cavity with also a nonresonant *back reflection* from the first mirror ($c = 1/\sqrt{2}$, $\varphi = \pi/4$, $\eta = 1/2$). From the phasor diagram [Fig. 2(b)] all the plots can be retrieved conveniently, by noticing that, from Eq. (2), the zero for Δ corresponds to the minimum of $\text{Re}(r)$ in the phase convention we take in Eq. (2).

The resonance parameters c, φ, η are bounded and related to each other by conservation of energy, which restricts the sum of the intensities at the output of all decay channels to be the same as the intensity at the input. For our formalism, this means that $|r|^2 \leq 1$. We allow $|r|$ to be less than one as we are considering also the presence of other channels that do not radiate to s_{out}. In general, one obtains a Fano lineshape for the reflected amplitude $|r|$, which can vary from a dispersive to absorptive (Lorentzian) shape depending on the value of φ. The Lorentzian lineshape is characteristic of relative phases between resonant and nonresonant channels that are 0 or π. The standard double-sided Fabry-Pérot cavity is an example, which has full transmission on resonance and large reflectance for large detuning. But in more complex systems also dispersive lineshapes can be encountered.

C. Measuring fluctuations: time-dependent output

We now demonstrate that, in the presence of a nonresonant channel, described by the first term on the rhs of Eq. (2), the measurement of cavity frequency fluctuations by means of a standard homodyne detection scheme is affected by the background contribution, represented in the equations by the dependence of the output signal from the parameters c and φ. This fact generally complicates the analysis of experimental data. We then present a method for eliminating this problem.

The effect of small modulation of cavity resonance frequency $\delta\omega_c$ is translated into the measured signal in the form of fluctuations of the homodyne output. In the presence of a modulation of the cavity frequency, the laser detuning Δ becomes time dependent

$$\Delta(t) = \bar{\Delta} + \delta\Delta(t) = \omega - \bar{\omega}_c - \delta\omega_c(t), \tag{6}$$

where $\delta\Delta$ and $\delta\omega_c$ denote the detuning and cavity resonance frequency fluctuations, and the horizontal bars denote mean values. In order to address mechanical fluctuations we want to measure the fluctuations of the homodyne signal $I_H(t) = \bar{I}_H + \delta I_H(t)$. The general expression for the output signal $I_H(t)$ from Eqs. (1) and (2) is

$$I_H = 4\eta\,|s_{\text{in}}|\,|s_{\text{lo}}| \left[c_n \sin(\varphi - \theta) + \frac{1}{1+\Delta_n^2}\left(\Delta_n \cos\theta + \sin\theta\right)\right]. \tag{7}$$

We are for now interested in small fluctuations and hence we linearize the response with respect to changes in the detuning parameter Δ, $\delta I_H = dI_H/d\Delta|_{\Delta_n=\bar{\Delta}_n} \times \delta\omega_c$ it follows that

$$\begin{aligned}\delta I_H(t) &= \frac{\delta\omega_c}{\kappa}\,|s_{\text{in}}|\,|s_{\text{lo}}|\,\frac{8\eta}{\left(1+\bar{\Delta}_n^2\right)^2} \\ &\quad\times\left[\left(1-\bar{\Delta}_n^2\right)\cos\theta - 2\bar{\Delta}_n\sin\theta\right] \\ &\equiv \frac{\delta\omega_c}{\kappa}\,|s_{\text{in}}|\,|s_{\text{lo}}|\,\beta(\bar{\Delta}_n,\eta,\theta),\end{aligned} \tag{8}$$

where we define the *transduction function*

$$\beta = \frac{8\eta}{\left(1+\bar{\Delta}_n^2\right)^2}\left[\left(1-\bar{\Delta}_n^2\right)\cos\theta - 2\bar{\Delta}_n\sin\theta\right] \tag{9}$$

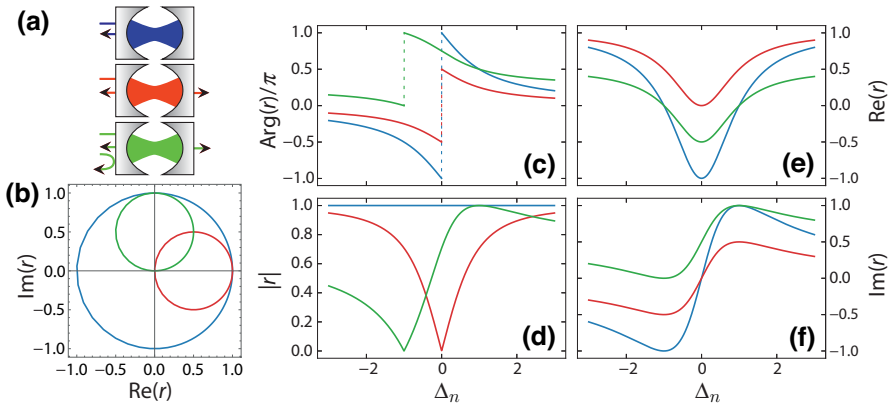

FIG. 2. (a) Three optical systems, i.e., Fabry-Pérot cavities with different coupling channels. In blue, the case of a single-sided cavity with only one resonant channel, in red, the case of a double-sided cavity with two resonant coupling channels, and in green, the case of a double-sided cavity plus a nonresonant channel. (b) The parametric plot shows the transfer function in the complex plane for the three cavities with the same color convention, whereas (c),(d) are the amplitude and phase of the complex transfer function versus laser detuning and (e),(f) its real and imaginary parts.

that defines how (normalized) frequency fluctuations in the cavity frequency are transduced into the detected homodyne signal (assuming linearization).

In order to access a particular quadrature of the signal s_{out}, ideally one would fix a value for the phase delay θ. In this case, the fluctuating signal $\delta I_H(t)$ would be independent on the background parameters c_n, φ, as one can see from Eq. (8). However, experimentally θ is not an accessible parameter and cannot be fixed directly. The measurement is accomplished, instead, by fixing the average output signal $\bar{I}_H$ to a constant value by introducing a feedback loop on the reference beam length (and hence phase ϕ_{lo}). The dramatic drawback consists of having δI_H dependent on the parameter c and φ through the phase θ.

For example, if we keep $\bar{I}_H = 0$ as is most conventionally done, we have

$$\theta(\bar{\Delta}_n) = \arctan\left(-\frac{\text{Im}(r)(\bar{\Delta}_n)}{\text{Re}(r)(\bar{\Delta}_n)}\right) + 2\pi n, \qquad (10)$$

where n is an integer. By using Eqs. (4) and (5) the ratio has an analytic form

$$-\frac{\text{Im}(r)}{\text{Re}(r)} = \frac{\bar{\Delta}_n + (1+\bar{\Delta}_n^2)c_n \sin\varphi}{1-(1+\bar{\Delta}_n^2)c_n\cos\varphi},$$

and hence we have that (modulo 2π)

$$\theta = \theta(\bar{\Delta}_n, c_n, \varphi) = \arctan\left(\frac{\bar{\Delta}_n + (1+\bar{\Delta}_n^2)c_n \sin\varphi}{1-(1+\bar{\Delta}_n^2)c_n\cos\varphi}\right).$$

If instead one would want to maximize the difference between the balanced detectors such that $\partial \bar{P}_H/\partial\theta = \text{Re}(r)(\bar{\Delta})\cos\theta - \text{Im}(r)(\bar{\Delta}_n)\sin\theta = 0$ one would obtain

$$\theta(\bar{\Delta}_n) = \arctan\left(\frac{\text{Re}(r)(\bar{\Delta}_n)}{\text{Im}(r)(\bar{\Delta}_n)}\right) + 2\pi n. \qquad (11)$$

This can be again written as above using Eqs. (4) and (5).

Hence using this scheme makes the homodyne angle θ dependent on the nonresonant parameters $\theta = \theta(\bar{\Delta}_n, c_n, \varphi)$. These expressions also vary with $\bar{\Delta}_n$ and as a result these settings do not necessarily probe the phase or amplitude quadrature for all laser frequencies. Moreover, if c and φ are not precisely known, even at detuning $\bar{\Delta} = 0$ the probed quadrature is not determined. As an example, consider the usual case of $\bar{I}_H = 0$. Then if $c = 0$, we have $\theta = \arctan(\Delta_n)$, which will probe the wanted quadrature $\theta = 0$, when $\Delta = 0$. (Hence, even in this ideal case we still need to know the detuning parameter separately.) However, taking into account the nonresonant channel means that even if we can separately set $\Delta = 0$ we will end up with $\theta = \arctan(c_n \sin\varphi/(1 - c_n\cos\varphi))$, which means that the transduction parameter will depend on the nonresonant channel.

All the above is not really a problem for the clear-cut cases where c, φ are known. However, especially for light interaction with complex nanophotonic systems such as photonic crystal cavities, to make quantitative predictions about the nonresonant reflection one should acquire knowledge about the optical setup configuration such as optical beam size and relative polarization between optical cavity mode and signal beam polarization [13]. The values of c and φ can vary from sample to sample and depend strongly on optical alignment. In fact, in the optomechanical devices based on photonic crystal cavities it is often impossible to measure c and φ as the reflectance $|r|$ as shown in Fig. 2 cannot be directly observed because of

large fluctuations and/or (optomechanical) nonlinearities [18,19].

D. Power spectral density

In a practical implementation, the output signal of the homodyne interferometer $I_H(t)$ is handled by an electronic spectrum analyzer, which measures the spectrum of fluctuations $\delta I_H(t)$ and quantifies these in terms of a (symmetrized) power spectral density.

We note that if two variables are linearly (and instantaneously) related via $x = ay$, their spectral densities are related through $S_{xx} = a^2 S_{yy}$. If we assume that the amplitude of the modulation $\delta\omega_c(t)$ is much smaller than the cavity linewidth κ, the variation of I_H can be approximated by the Taylor expansion truncated to first order: $\delta I_H = (\partial \bar{I}_H/\partial\bar{\omega}_c)\delta\omega_c$, as we did in Eq. (8). In this case it is possible to write an analytical expression for the transduction from a given fluctuation spectrum of ω_c to I_H: the spectral density of the frequency fluctuations $S_{\omega\omega}$ is related to the measured signal from the spectrum analyzer $S_{I_H I_H}$, by means of the relationship [24]

$$S_{I_H I_H}(\Omega) = \frac{\beta^2}{\kappa^2}\frac{P_{\rm in}P_{\rm lo}}{(\hbar\omega_l)^2}S_{\omega\omega}(\Omega), \tag{12}$$

where the *transduction function* β is introduced in Eq. (8)

$$\beta^2(\bar{\Delta}_n,\eta,\theta) = \frac{64\eta^2}{(1+\bar{\Delta}_n^2)^4} \times\left[(1-\bar{\Delta}_n^2)\cos(\theta) - 2\bar{\Delta}_n\sin(\theta)\right]^2 \tag{13}$$

and we assume $\theta = \theta(\bar{\Delta}_n, c_n, \varphi)$ due to the way the homodyne is locked.

Figures 3 and 4 show the transduction function β^2 for the three types of cavities depicted in Fig. 2, with the assumption that the homodyne is locked by either minimizing (Fig. 3) or maximizing (Fig. 4) $|I_H|$. All figures have been normalized by dividing Eq. (13) by 64 (so that the maximum with $\eta = 1$ is one). From these figures, we see that the shape of the transduction function can vary considerably depending on the nonresonant parameters, making the experimental results hard to interpret, especially if c and φ are not well controlled.

III. QUADRATURE-AVERAGED HOMODYNE DETECTION

We now show that introducing a periodic modulation on the reference beam phase leads to a result that is closer to the ideal homodyne detection, from the point of view that the dependence of θ on the nonresonant scattering parameters is erased. This in turn implies that the measurement probes only the resonant channel of the optical system, described by the second term of Eq. (2).

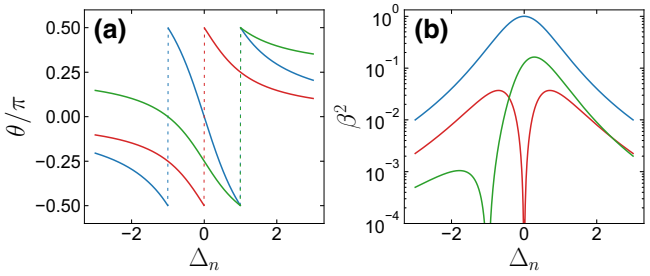

FIG. 3. Transduction function versus laser detuning when $|\bar{I}_H|$ is minimized. Panel (a) shows the effective homodyne angle and panel (b) the β^2 parameter. The different colors correspond to the three cavities shown in Fig. 2: single-sided cavity (blue), double-sided cavity (red), and double-sided cavity with a nonresonant channel (green).

We assume that the phase difference between the signal and local oscillator is now harmonically modulated in time $\theta = 2\pi\nu t$ and that the time of acquisition is sufficiently large (meaning that the signal is collected over multiple periods of modulation), so that we can average $\langle\delta I_H^2\rangle$ over time. Using Eq. (13) and

$$\begin{aligned}
\int_\tau dt\cos^2(2\pi\nu t) &= \frac{1}{2\pi}\int_0^{2\pi} d\theta\cos^2\theta = \frac{1}{2}\\
\int_\tau dt\sin^2(2\pi\nu t) &= \frac{1}{2\pi}\int_0^{2\pi} d\theta\sin^2\theta = \frac{1}{2}\\
\int_\tau dt\sin(2\pi\nu t)\cos(2\pi\nu t) &= \frac{1}{2\pi}\int_0^{2\pi} d\theta\sin\theta\cos\theta = 0,
\end{aligned} \tag{14}$$

we arrive at an expression for the transduction of the form

$$\boxed{\beta^2_{\rm QA}(\bar{\Delta},\eta) = \frac{32\eta^2}{\left(1+\bar{\Delta}_n^2\right)^2}}. \tag{15}$$

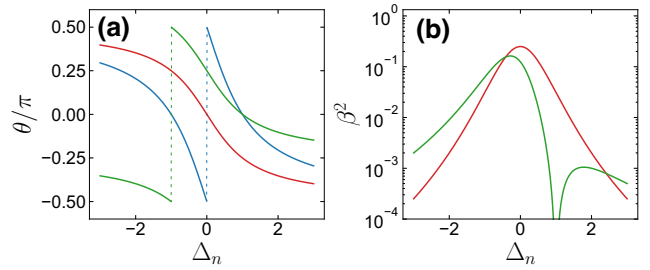

FIG. 4. Transduction function versus laser detuning when $|\bar{I}_H|$ is maximized. Panel (a) shows the effective homodyne angle and panel (b) the β^2 parameter. The different colors correspond to the three cavities shown in Fig. 2: single-sided cavity (blue), double-sided cavity (red), and double-sided cavity with a nonresonant channel (green). Note that the single-sided cavity β is now identically zero and hence not shown.

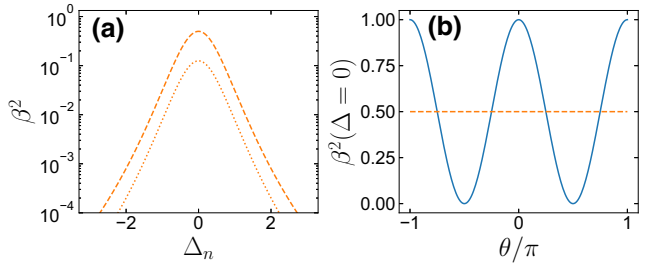

FIG. 5. (a) Transduction function for quadrature-averaged homodyne detection. The dashed line assuming $\eta = 0.5$ and the dotted line with $\eta = 1$. (b) Comparison between transduction function for single-quadrature and quadrature-averaged measurements versus angle θ for $\bar{\Delta} = 0$, when $\eta = 1, c = 1, \varphi = 0$. At every angle the quadrature averaged measurement is at most a factor of 2 less sensitive.

The transduction now has a simple dependence on the cavity resonance parameters and by fitting the experimental data across all laser frequencies with two parameters it is possible to characterize the cavity resonance. In Fig. 5 we show the β_{QA} that now assumes the same detuning dependence for all the cases depicted in Fig. 2. This has to be compared with the result of Figs. 3 and 4 already discussed.

The drawback of this method is a decreased sensitivity but that amounts to a maximum factor of 2 with respect to the ideal case. In Fig. 5 we show that the sensitivity of the measurement in the quadrature-averaged case is indeed decreased by at most a factor of 3 dB. In order to do so we compare the case of a single-sided Fabry-Pérot cavity for which the sensitivity is maximum, at $\Delta = 0$. The maximum sensitivity that follows from Eq. (13) is

$$\beta(\bar{\Delta} = 0) = 64\eta^2 \cos^2\theta = 2\cos^2\theta\beta_{\mathrm{QA}}(\Delta = 0), \quad (16)$$

from which it follows that the decrease in the sensitivity happens for $\theta = n\pi$ (with n integer), that corresponds to phase quadrature.

One could notice that the way we operate the homodyne interferometer here would correspond to performing an heterodyne detection with a negligible frequency difference between the two beams of the interferometer, hence we could call this technique "dc-heterodyne detection." Hence, the decreased sensitivity compared to a "pure" homodyne configuration can be explained as a fundamental limitation deriving from signal-to-noise limitation of a heterodyne detector.

IV. CHARACTERIZATION OF ABSOLUTE MAGNITUDE OF MODULATION

In the previous section we show that, by averaging the output signals over the different field quadratures, we obtain a simple expression for the transduction β, that describes how the fluctuations of a cavity frequency transform the output signal of our homodyne interferometer. Of note, we make the approximation that the amplitude of the cavity frequency modulation $\delta\omega$ is small compared to the cavity linewidth κ and we consider only the first term in the Taylor expansion of the output signal I_H. Our function β_{QA} is relative to the *linear transduction* of the modulation $\delta\omega$ since it transforms a modulation signal on the cavity frequency in the homodyne output, in a linear fashion. By retaining only the linear term, we discard the nonlinear part of I_H, losing precious information about our system. Now, while considering the case of harmonic modulation at a frequency Ω: $\delta\omega = A\cos(\Omega t)$, we show how one can use the information contained in nonlinear part of I_H in order to make predictions on the modulation amplitude A [19].

We can write the full Taylor expansion of $I_H(t)$ as

$$\begin{aligned} I_H(t) &= \sum_{k=0}^{\infty} \frac{1}{k!} \frac{\partial^k I_H(\bar{\Delta})}{\partial \Delta^k} [\delta\omega(t)]^k \\ &= \sum_k \frac{1}{k!} \frac{\partial^k I_H}{\partial \Delta^k} [A\cos(\Omega t)]^k . \end{aligned} \quad (17)$$

Since we still want to consider the case of small modulation amplitudes: $A \ll \kappa$, it is possible to make the following "order-by-order" approximation [19,25,26]

$$\cos^k(\Omega t) \simeq \frac{1}{2^{k-1}} \cos(k\Omega t), \quad (18)$$

since, when A is small, the convergence of the sum is ensured by cutting the sum index to a finite value. The relationship in Eq. (18) makes it possible to immediately write $I(t)$ as a Fourier series

$$I_H(t) = \sum_k \frac{1}{k!} \frac{\partial^k I_H}{\partial \Delta^k} \frac{A^k}{2^{k-1}} \cos(k\Omega t) = \sum_k I_k(t). \quad (19)$$

At this point one can exploit the same method already used for the derivation of β_{QA}, in order to define an expression of the transduction correspondent to each kth order in Ω, $\beta_{\mathrm{QA},k}$. In particular, the operator $\beta_{\mathrm{QA},k}$ is defined by an analogous relationship as in Eq. (12), by noticing that every term $I_k(t)$ is linear in $\cos(k\Omega t)$.

In order to derive an expression for the transduction, we need to evaluate $\beta^2_{\mathrm{QA},k} = \left\langle \left[\partial^k I_H/\partial\Delta^k\right]^2 \right\rangle_\theta$

$$\begin{aligned} \left\langle \left[\frac{\partial^k I_H}{\partial \Delta^k}\right]^2 \right\rangle_\theta &= (-4\eta\,|s_{\mathrm{in}}|\,|s_{\mathrm{lo}}|)^2 \\ &\times \left\langle \left[\frac{\partial^k}{\partial\Delta^k}\left(\frac{\Delta_n}{1+\Delta_n^2}\cos\theta - \frac{1}{1+\Delta_n^2}\sin\theta\right)\right]^2 \right\rangle_\theta \\ &= 8(\eta\,|s_{\mathrm{in}}|\,|s_{\mathrm{lo}}|)^2 \left[\left(\frac{\partial^k}{\partial\Delta^k}\frac{\Delta_n}{1+\Delta_n^2}\right)^2 + \left(\frac{\partial^k}{\partial\Delta^k}\frac{1}{1+\Delta_n^2}\right)^2\right], \end{aligned} \quad (20)$$

where in the last line we perform the averaging over all angles θ as previously.

For simplifying notation, we mark $f = \Delta_n/(1+\Delta_n^2)$, $g = 1/(1+\Delta_n^2)$, and $\partial^k = \partial^k/\partial\Delta^k$. We then have to solve for $(\partial^k f)^2$ and $(\partial^k g)^2$. Since they are both real valued we can write

$$(\partial^k f)^2 + (\partial^k g)^2 = (\partial^k f + i\partial^k g)(\partial^k f - i\partial^k g). \quad (21)$$

At this point it is possible to write an expression for the kth-order derivative of both f and g. Indeed, in view of linearity of the derivative we can write

$$\begin{aligned}\frac{\partial^k}{\partial\Delta^k}(f+ig) &= \frac{\partial^k}{\partial\Delta^k}\left(\frac{\Delta_n+i}{1+\Delta_n^2}\right)\\ &= \frac{\partial^k}{\partial\Delta^k}\frac{1}{\Delta_n - i}\\ &= \left(\frac{-2}{\kappa}\right)^k \frac{k!}{(\Delta_n - i)^{k+1}}\end{aligned}$$

and in the same way

$$\frac{\partial^k}{\partial\Delta^k}(f-ig) = \left(\frac{-2}{\kappa}\right)^k \frac{k!}{(\Delta_n + i)^{k+1}}.$$

Equation (21) then becomes

$$(\partial^k f)^2 + (\partial^k g)^2 = \left(\frac{-2}{\kappa}\right)^{2k} \frac{(k!)^2}{(\Delta_n^2+1)^{k+1}},$$

and this ultimately implies that

$$\left\langle\left[\frac{\partial^k I_H}{\partial\Delta^k}\right]^2\right\rangle_\theta = 8\eta^2\frac{P_{\rm in}P_{\rm lo}}{(\hbar\omega_l)^2}\left(\frac{2}{\kappa}\right)^{2k}\frac{(k!)^2}{(\Delta_n^2+1)^{k+1}}.$$

We can call $S_{I_kI_k}$ the PSD of the kth term in Eq. (19) and $S_{\Omega_k\Omega_k}$ the δ function correspondent to the $\cos(k\Omega t)$, so that

$$\begin{aligned}S_{I_kI_k} &= \beta_{{\rm QA},k}^2\frac{P_{\rm in}P_{\rm lo}}{(\hbar\omega_l)^2}S_{\Omega_k\Omega_k}\\ &= \beta_{{\rm QA},k}^2\frac{P_{\rm in}P_{\rm lo}}{(\hbar\omega_l)^2}\delta(\Omega-\Omega_k).\end{aligned} \quad (22)$$

Note that we now include the κ term inside β unlike in Eq. (13). From Eqs. (19) and (22) it then follows that

$$\boxed{\beta_{{\rm QA},k}^2 = \left(\frac{A}{\kappa}\right)^{2k}\frac{32\eta^2}{(1+\Delta_n^2)^{k+1}}.} \quad (23)$$

From Eq. (23) one can see that by comparing the relative weights of the different harmonic components we can arrive at an estimate of A that is independent of constant terms such as the powers $P_{\rm in}, P_{\rm lo}$ or the coupling factor η. For example, if we look at the ratio of the higher-order modulation with respect to the lower order at zero detuning

$$\left.\frac{S_{I_{k+1}I_{k+1}}}{S_{I_kI_k}}\right|_{\bar\Delta=0} = \left.\frac{\beta_{{\rm QA},k+1}}{\beta_{{\rm QA},k}}\right|_{\bar\Delta=0} = \left(\frac{A}{\kappa}\right)^2, \quad (24)$$

we see that there is a straightforward connection to the *modulation strength* defined as the ratio between the modulation amplitude and the cavity linewidth A/κ. This is enforced by the fact that contrarily to the standard case, in the quadrature-averaged case, the transduction peaks at $\Delta = 0$ at all the orders.

For large modulations $A \simeq \kappa$, the approximation in Eq. (18) is no longer valid, and one cannot exploit this method. In this case it is only possible to give a numerical estimate of the shape of the transduction operator for the higher orders since we cannot anymore exploit the convergence of the truncated Taylor expansion valid for small perturbations.

V. EXPERIMENTAL DEMONSTRATION

To compare the above formulation to experiments, we perform measurements on a sliced photonic crystal nanobeam resonator [18,19] using both the "locked homodyne" method (with absolute value of the dc photocurrent minimized) and the "swept homodyne" method presented above. The results are analyzed in Fig. 6 where the area under the mechanical resonance peak is plotted as a function of the laser wavelength, together with the bare spectrograms. The experiments are performed in a room-temperature vacuum chamber (where the temperature and vacuum pressure are constant) with a focused laser beam incident from free space at normal incidence to the sample and measured in reflection, and with a constant laser power so that the variation in the measured signal as a function of the wavelength is solely due to variation of the transduction parameter β in Eq. (15). As expected, our data shows that whereas the swept homodyne case produces a well-defined single resonance from which the optical cavity properties can be extracted [$\kappa/(2\pi) \approx 184$ GHz], the locked homodyne shows a distinct Fano shape, that is significantly harder to interpret and can even lead to a significant underestimation for the cavity linewidth if not properly analyzed.

In Fig. 7 similar data is presented for the second-order peak. Similarly as in the first-order case, sweeping the homodyne phase turns the Fano shape into a simple peak. More interestingly, from this data we can extract the ratio of the signal from the second-order peak to the first order, which turns out to be approximately 0.023. This corresponds to ratio A/κ of 0.15 according to Eq. (23). Assuming that the amplitude of the frequency fluctuations follows $A = 2\delta\omega_{\rm rms} = 2\sqrt{2n_{\rm th}}g_0$ [where $n_{\rm th} = k_BT/(\hbar\omega_m)$]

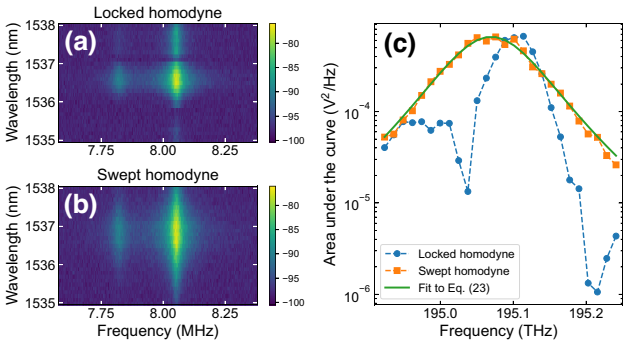

FIG. 6. Spectrograms for the locked homodyne (a) and swept homodyne (b) measurement for the first-order mechanical signal. The colorscale shows the measured voltage signal (I_H after a transimpedance amplifier) in dB scale. Panel (c) shows the integrated area under the mechanical signal peak as a function of laser detuning, together with a fit to Eq. (23) for the swept homodyne data. The lower frequency signal is another mechanical mode that we do not consider here.

and using $\kappa/(2\pi) = 184$ GHz extracted above, we get that $g_0/(2\pi) \approx 11$ MHz, which is well in line with the parameters we extract before for similar resonators using independent methods.

VI. CONCLUSIONS AND DISCUSSION

In conclusion, we show both theoretically and numerically that averaging a homodyne interferometer over all possible measurement angles can have advantages in specifically estimating the parameters of resonant cavities when both resonant and nonresonant signals are present. Although this is especially acute in cavity-optomechanical systems utilizing nanophotonic cavities, we speculate that our method could find application also in other areas where sensing of harmonically modulated signals is useful. Besides modulations of mechanical origin, such signals could be related to rf fields through electro-optic interaction or weak optical signals through optical nonlinearities. Moreover, it could be interesting to investigate the use of our method on cavity-enhanced frequency modulation spectroscopy [27,28], which is employed for various optical sensing applications, in cases where the used cavities exhibit Fano resonances.

Additionally, we point out the fact that the homodyne interferometer angle can depend very sensitively on the detuning and nonresonant parameters. We think this is an underappreciated feature that should be considered carefully in experiments. Fortunately, the averaging presented here can remedy this problem.

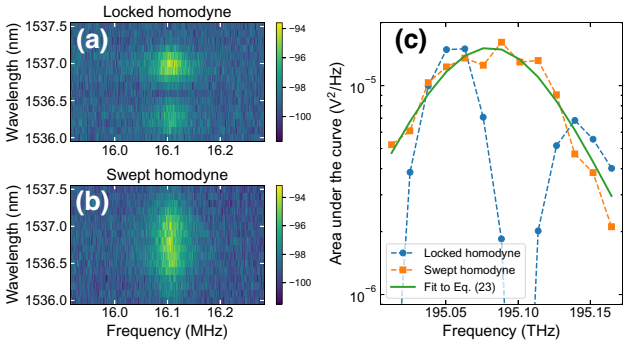

FIG. 7. Spectrograms for the locked homodyne (a) and swept homodyne (b) measurement for the second-order mechanical signal. The colorscale shows the measured voltage signal (I_H after a transimpedance amplifier) in dB scale. Panel (c) shows the integrated area under the mechanical signal peak as a function of laser detuning, together with a fit to Eq. (23) for the swept homodyne data.

ACKNOWLEDGMENTS

We thank Amy Navarathna for assistance in sample fabrication. This project has received funding from the European Research Council (ERC) under the European Union's Horizon 2020 research and innovation programme (Grant Agreements No. 852428 and No. 759644) and from Academy of Finland Grant No. 321416. This work is part of the research programme of the Netherlands Organisation for Scientific Research (NWO), and supported by an NWO Vidi grant.

APPENDICES

APPENDIX: THE EFFECTS OF NONIDEAL AVERAGING

In deriving Eq. (15) we assume a perfect averaging over the quadrature angles so that $\cos^2\theta$ and $\sin^2\theta$ average to 1/2 and $(\sin\theta\cos\theta)$ to 0. A reasonable concern is that in experiments the averaging is never perfectly over an exact number of full cycles. However, as we show below, as long as one averages even only a couple of full cycles of θ, the error in β^2 becomes small, irrespective if the averaging is done over an integer number of cycles.

In order to calculate the error we need to calculate the averages for the sine and cosine terms at arbitrary values of averaging time $\varphi = \omega t$

$$\frac{1}{\varphi}\int_0^{\varphi} dx\,\cos^2(x) = \frac{1}{2} + \frac{\sin(2\varphi)}{4\varphi},$$
$$\frac{1}{\varphi}\int_0^{\varphi} dx\,\sin^2(x) = \frac{1}{2} - \frac{\sin(2\varphi)}{4\varphi},$$
$$\frac{1}{\varphi}\int_0^{\varphi} dx\,\sin(x)\cos(x) = \frac{\sin^2(\varphi)}{2\varphi},$$

from which one can see that the envelope of the averaging error gets smaller with $1/\varphi$ as could be expected. We can make this more quantitative by inputting these equations

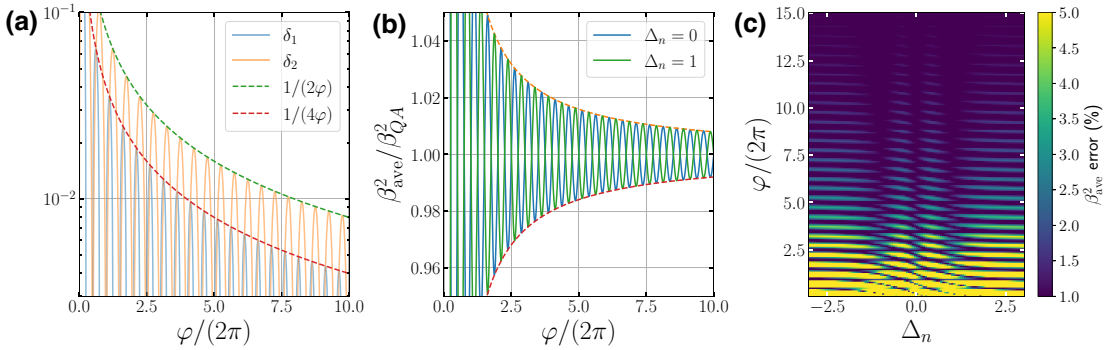

FIG. 8. Averaging errors. Panel (a) shows the value of δ_1 and δ_2 (defined in main text) as a function of the total averaging angle φ. Panel (b) depicts the relative error in the parameter β^2 as a function of φ and panel (c) shows the relative error in β^2 as a function of both φ and normalized detuning Δ_n. Note that the colorbar is cut so that all values above 5 % show yellow and values below 1 % dark blue.

now to Eq. (13)

$$\beta^2_{\rm ave}(\bar{\Delta}_n,\eta,\varphi) = \frac{64\eta^2}{(1+\bar{\Delta}_n^2)^4} \times\Big[(1-\bar{\Delta}_n^2)^2\left(\frac{1}{2}+\delta_1(\varphi)\right)+4\bar{\Delta}_n^2\left(\frac{1}{2}-\delta_1(\varphi)\right) -4\Delta_n(1-\Delta_n^2)\delta_2(\varphi)\Big],$$

where we mark

$$\delta_1(\varphi) = \frac{\sin(2\varphi)}{4\varphi},$$

$$\delta_2(\varphi) = \frac{\sin^2(\varphi)}{2\varphi}.$$

These are plotted in Fig. 8(a).

In Fig. 8(b) we then plot the ratio between this averaged value and the ideal case $\beta^2_{\rm ave}(\bar{\Delta}_n,\eta,\varphi)/\beta^2_{\rm QA}(\bar{\Delta},\eta)$ at a couple of different detunings Δ_n. From this we can readout that to get below 5 % error in the β^2 parameter, averaging over only two full cycles is enough at these detunings. To get below 1 % error, one needs to average over eight full cycles. Finally in Fig. 8(c) we plot the same plot for all detunings.

[1] B. P. Abbott, (LIGO Scientific Collaboration and Virgo Collaboration), Gw150914: The Advanced LIGO Detectors in the Era of First Discoveries, Phys. Rev. Lett. **116**, 131103 (2016).

[2] M. Aspelmeyer, T. J. Kippenberg, and F. Marquardt, Cavity optomechanics, Rev. Mod. Phys. **86**, 1391 (2014).

[3] H.-A. Bachor and T. C. Ralph, *A Guide to Experiments in Quantum Optics* (Wiley-VCH, Weinheim, 2019), 3rd ed.

[4] A. I. Lvovsky and M. G. Raymer, Continuous-variable optical quantum-state tomography, Rev. Mod. Phys. **81**, 299 (2009).

[5] D. Jackson, A. Kersey, M. Corke, and J. Jones, Pseudo-heterodyne detection scheme for optical interferometers, Electron. Lett. **18**, 1081 (1982).

[6] Y. Sasaki and H. Sasaki, Heterodyne detection for the extraction of the probe-scattering signal in scattering-type scanning near-field optical microscope, Jpn. J. Appl. Phys. **39**, L321 (2000).

[7] R. Hillenbrand and F. Keilmann, Complex Optical Constants on a Subwavelength Scale, Phys. Rev. Lett. **85**, 3029 (2000).

[8] N. Ocelic, A. Huber, and R. Hillenbrand, Pseudoheterodyne detection for background-free near-field spectroscopy, Appl. Phys. Lett. **89**, 101124 (2006).

[9] M. Munroe, D. Boggavarapu, M. E. Anderson, and M. G. Raymer, Photon-number statistics from the phase-averaged quadrature-field distribution: Theory and ultrafast measurement, Phys. Rev. A **52**, R924 (1995).

[10] D. F. McAlister and M. G. Raymer, Ultrafast photon-number correlations from dual-pulse, phase-averaged homodyne detection, Phys. Rev. A **55**, R1609 (1997).

[11] A. I. Lvovsky, H. Hansen, T. Aichele, O. Benson, J. Mlynek, and S. Schiller, Quantum State Reconstruction of the Single-Photon Fock State, Phys. Rev. Lett. **87**, 050402 (2001).

[12] M. Aspelmeyer, T. J. Kippenberg, and F. Marquardt, Cavity optomechanics, Rev. Mod. Phys. **86**, 1391 (2014).

[13] M. Galli, S. L. Portalupi, M. Belotti, L. C. Andreani, L. O'Faolain, and T. F. Krauss, Light scattering and Fano resonances in high-Q photonic crystal nanocavities, Appl. Phys. Lett. **94**, 071101 (2009).

[14] A. E. Miroshnichenko, S. Flach, and Y. S. Kivshar, Fano resonances in nanoscale structures, Rev. Mod. Phys. **82**, 2257 (2010).

[15] B.-B. Li, Y.-F. Xiao, C.-L. Zou, Y.-C. Liu, X.-F. Jiang, Y.-L. Chen, Y. Li, and Q. Gong, Experimental observation of Fano resonance in a single whispering-gallery microresonator, Appl. Phys. Lett. **98**, 021116 (2011).

[16] D. Ding, M. J. A. de Dood, J. F. Bauters, M. J. R. Heck, J. E. Bowers, and D. Bouwmeester, Fano resonances in a

multimode waveguide coupled to a high-Q silicon nitride ring resonator, Opt. Express **22**, 6778 (2014).

[17] G. Zhao, T. Zhao, H. Xiao, Z. Liu, G. Liu, J. Yang, Z. Ren, J. Bai, and Y. Tian, Tunable Fano resonances based on microring resonator with feedback coupled waveguide, Opt. Express **24**, 20187 (2016).

[18] R. Leijssen and E. Verhagen, Strong optomechanical interactions in a sliced photonic crystal nanobeam, Sci. Rep. **5**, 15974 (2015).

[19] R. Leijssen, G. R. La Gala, L. Freisem, J. T. Muhonen, and E. Verhagen, Nonlinear cavity optomechanics with nanomechanical thermal fluctuations, Nat. Commun. **8**, 16024 (2017).

[20] M. F. Limonov, M. V. Rybin, A. N. Poddubny, and Y. S. Kivshar, Fano resonances in photonics, Nat. Photonics **11**, 543 (2017).

[21] A. Naesby and A. Dantan, Microcavities with suspended subwavelength structured mirrors, Opt. Express **26**, 29886 (2018).

[22] H. A. Haus, *Waves and Fields in Optoelectronics* (Prentice-Hall, Englewood Cliffs, N.J., 1984).

[23] U. Fano, Effects of configuration interaction on intensities and phase shifts, Phys. Rev. **124**, 1866 (1961).

[24] M. L. Gorodetsky, A. Schliesser, G. Anetsberger, S. Deleglise, and T. J. Kippenberg, Determination of the vacuum optomechanical coupling rate using frequency noise calibration, Opt. Express. **18**, 23236 (2010).

[25] B. Hauer, J. Maciejko, and J. Davis, Nonlinear power spectral densities for the harmonic oscillator, Ann. Phys. (N. Y) **361**, 148 (2015).

[26] G. A. Brawley, M. R. Vanner, P. E. Larsen, S. Schmid, A. Boisen, and W. P. Bowen, Nonlinear optomechanical measurement of mechanical motion, Nat. Commun. **7**, 10988 (2016).

[27] G. C. Bjorklund, Frequency-modulation spectroscopy: A new method for measuring weak absorptions and dispersions, Opt. Lett. **5**, 15 (1980).

[28] O. Axner, P. Ehlers, A. Foltynowicz, I. Silander, and J. Wang, in *Cavity-Enhanced Spectroscopy and Sensing*, Springer Series in Optical Sciences, edited by G. Gagliardi and H.-P. Loock (Springer, Berlin, Heidelberg, 2014), p. 211.